Physica 106B (1981) 33–46
North-Holland Publishing Company

THE ac IMPEDANCE OF ELECTRO–ACOUSTICALLY ACTIVE CdS

W. WESTERA and R. J. J. ZIJLSTRA
Fysisch Laboratorium, Rijksuniversiteit Utrecht, The Netherlands

Received 25 September 1980

The ac impedance of electro–acoustically active semiconductors is calculated and measured. The need for nonlinear equations is avoided by the assumption that the observed electro–acoustic effects can be described by the trapping of bunches of free charge carriers in potential troughs which are coupled to the amplified acoustic waves. The potential troughs are created and annihilated at random throughout the crystal. The creation rate and annihilation rate of the troughs are essentially electric field dependent. Furthermore, the effects of the displacement current, the diffusion current, the space charge, and anisotropy are taken into account. Measurements of the ac impedance between 0.5 and 100 MHz made on single crystals of semiconducting CdS are in good agreement with the calculations. The impedances show a low frequency roll-off (1 MHz) and resonances that are related to the transit time of potential troughs.

1. Introduction

Amplification of travelling acoustic waves as a result of interaction with supersonic drifting charge carriers in piezoelectric semiconductors, i.e. the electro-acoustic effect, has been a subject of continuous interest for many years. An ultrasonic wave which propagates in a piezoelectric semiconductor will be accompanied by a piezoelectric field which in turn acts on the mobile charge carriers. While the establishment of a space charge wave is a pre-requisite for the existence of coupling between charge carriers and an acoustic wave, it is apparent that the interaction vanishes at high frequencies through diffusion and at low frequencies through the dielectric relaxation mechanism. It follows therefore that optimum amplification is obtained at frequencies determined by the angular diffusion frequency ω_D and the angular dielectric relaxation frequency ω_C. After the first experimental results of ultrasonic amplification in CdS were reported in 1961 by Hutson et al. [1], White [2] in 1962 gave a linear description of the electro-acoustic effect, known as the linear small signal gain theory. White did in fact find the frequency of maximum amplification to be $\omega_m = (\omega_C \omega_D)^{\frac{1}{2}}$; in all piezoelectric semiconductors this value lies in the GHz-range.

From Brillouin scattering- [3], microwave emission- [4], and sound-amplification [1] data it is known that the amplification process can only be described by the linear small-signal gain theory at low acoustic flux intensities. At higher acoustic flux intensities, or rather at higher electric field strengths, many non-linear effects become important; these include parametric interaction of acoustic waves, current saturation, large current fluctuations, electro–acoustic domain formation, impedance effects and so on, which cannot be described by linear theories. We must bear in mind that the large current fluctuations and the impedance effects appear at low frequencies (MHz range). Several authors [5, 6] have tried to describe these phenomena. Since however it is very difficult to describe these non-linear effects, when starting from basic principles, many of these phenomena are not yet understood quantitatively.

In 1967 Moore [7] avoided the need to use non-linear equations by suggesting that the observed current saturation and current fluctuations are caused by bunching of free charge carriers in potential troughs, which are coupled to the amplified acoustic waves via the piezoelectric effect. He described the observed current fluctuations in CdS by a trough creation–annihilation process.

In 1978 Zijlstra and Gielen [8] modified this theory by accounting for transit time effects in a local

0378-4363/81/0000–0000/$2.50

description. They neglected the displacement and the diffusion current in the expression for the current density and assumed that the creation and the annihilation of troughs are independent of electric field strength. Their calculation resulted in a frequency-independent impedance. Experimentally, however, the observed ac impedance of electro–acoustically active CdS crystals turned out to be frequency dependent [9]. In fact experimental results showed that in addition to the familiar dielectric roll-off, there was another, lower frequency roll-off in the range of 1 MHz.

In 1965 Greebe [10] used the linear small-signal theory to calculate the effects, that boundary conditions have on the impedance of semiconducting piezoelectric plates. His results, however, were not applicable to electro–acoustically active semiconductors.

The aim of this paper is to show that the observed frequency dependence of the ac impedance can be explained if the local description is extended by taking into account diffusion, space charge, displacement current, the electric field dependence of the trough creation and annihilation rates [11], and by allowing for off-axis waves. It should be noted that this calculation holds for crystals where a continuous type of amplified acoustic flux is observed (i.e. where no travelling electro–acoustic domains are observed).

2. Theory

In this chapter we calculate the ac impedance of an electro–acoustically active semiconducting crystal, starting from the trough model. It is assumed that on the time scale considered the free carrier collision time is small and that the mean free path of free charge carriers is much smaller than the wavelengths involved in the sound amplification process. Under these conditions one can use a classical continuum description. Furthermore, anisotropy effects are taken into account.

2.1. Basic equations

We consider an n-type homogeneous piezoelectric semiconducting crystal, where the electric field is applied along a symmetry axis, the x_3-axis. In the case of CdS the x_3-axis coincides with the c-axis. Together with the x_1 and x_2-axis the x_3-axis forms a cartesian coordinate system. The sample is supplied with ohmic contacts at $x_3 = 0$ and $x_3 = L$, where L is the contact spacing.

When the drift velocity of the electrons v_d exceeds the sound velocity v_s, travelling acoustic waves are amplified from the thermal background. As a result of the interference of the amplified acoustic waves, potential troughs which propagate with the sound velocity in the direction of the anode, are spontaneously created and annihilated throughout the crystal. Note that the creation and annihilation occurs at random as a result of the incoherent input of the amplification process, i.e. the thermal phonon distribution.

As it is known from the literature [12], that under these conditions it is transverse off-axis waves which are amplified rather than longitudinal on-axis waves, our calculation must describe the anisotropic propagation characteristics of acoustic waves and the anisotropy of the piezoelectric and dielectric properties as well. We shall consider off-axis sound waves and indicate how the general form of the piezoelectric relations and the wave equation can be reduced to the simple one-dimensional form (cf. [13]).

In the analyses given below we used the sign convention, when $E < 0$ and $I < 0$, then $V > 0$, where V is the applied voltage, E the electric field strength and I the electric current.

Let n_d and n_s be the local densities of the free and trapped electrons in the conduction band and let n be the total electron density in that band; then

$$n = n_d + n_s. \tag{1}$$

Gauss's equation yields

$$\frac{\partial D_i}{\partial x_i} = -q(n - \bar{n}), \tag{2}$$

where D_i is the ith component of the dielectric displacement, x the position, $-q$ the electron charge. The time average of n is denoted by $\bar{n}$ and is assumed to be equal to the thermal equilibrium density of free carriers; i is a subscript running from 1 to 3. It should be noted that we have to carry out summation over repeated subscripts (Einstein convention). The total current density equation becomes

$$j_i = -qn_d v_{d_i} - qn_s v_{s_i} + qD_{n_{ij}} \frac{\partial n}{\partial x_j} + \frac{\partial D_i}{\partial t}, \tag{3}$$

where $\boldsymbol{j}$ is the total current density, $D_{n_{ij}}$ a tensor describing the anisotropic diffusion, t is time, v_d and v_s are the drift velocities of free and trapped electrons, respectively. (Note that $\bar{v}_s$ is equal to the sound velocity.) In addition, we have, since $\boldsymbol{j}$ is solenoidal

$$\frac{\partial j_i}{\partial x_i} = 0, \tag{4}$$

the piezoelectric relations

$$T_{ij} = c_{ijkl} S_{kl} - e_{kij} E_k, \tag{5}$$

$$D_i = \epsilon_{ij} E_j + e_{ijk} S_{jk}, \tag{6}$$

Newton's second law

$$\frac{\partial T_{ik}}{\partial x_k} = \rho \frac{\partial^2}{\partial t^2} u_i, \tag{7}$$

and

$$S_{ij} = \frac{1}{2}\left(\frac{\partial u_i}{\partial x_j} + \frac{\partial u_j}{\partial x_i}\right), \tag{8}$$

where T_{ij} and S_{ij} are stress and strain tensor elements, respectively, whereas c_{ijkl}, e_{ijk} and ϵ_{ij} are the elastic, piezoelectric and dielectric tensor elements, respectively. $\boldsymbol{E}$ is the electric field strength vector, ρ the mass density and $\boldsymbol{u}$ the displacement vector.

When p and b are the creation and annihilation rate of troughs per unit volume, respectively, the master equation for the trough density n_t reads:

$$\frac{\partial n_t}{\partial t} = p - b - v_{s_i} \frac{\partial n_t}{\partial x_i}. \tag{9}$$

In addition we make the approximation that each trough contains N electrons, where N does not depend explicitly on $\boldsymbol{x}$. Then the density of trapped electrons becomes

$$n_s = N n_t. \tag{10}$$

2.2. The stationary state

If we realize that the electric field strength is applied along the x_3-axis, we have

$$\frac{\partial \bar{E}_k}{\partial x_j} = 0, \quad \text{unless } k = j = 3. \tag{11}$$

Because of the symmetry it is reasonable to assume that the static displacement and strain components, $\bar{u}_i$ and $\bar{S}_{ij}$ depend only on x_3. Therefore we obtain (cf. eq. (8)):

$$\bar{S}_{ij} = 0, \quad \text{unless } i = 3 \text{ or } j = 3,$$

$$\frac{\partial \bar{S}_{ij}}{\partial x_k} = 0, \quad \text{unless } k = 3. \tag{12}$$

In the stationary state eq. (7) yields

$$\frac{\partial \bar{T}_{ij}}{\partial x_j} = 0. \tag{13}$$

With the help of eqs. (5) and (13) we find

$$c_{ijkl} \frac{\partial \bar{S}_{kl}}{\partial x_j} - e_{kij} \frac{\partial \bar{E}_k}{\partial x_j} = 0. \tag{14}$$

Since it is known that in the case of crystals with a hexagonal symmetry, such as those of CdS, $c_{333k} = 0$ and $c_{33k3} = 0$ unless $k = 3$, eq. (14) becomes when $i = 3$ with the help of eqs. (11) and (12):

$$\frac{\partial \bar{E}_3}{\partial x_3} = \frac{c_{3333}}{e_{333}} \frac{\partial \bar{S}_{33}}{\partial x_3}. \tag{15}$$

From eqs. (2) and (6) we find

$$\epsilon_{ij} \frac{\partial \bar{E}_j}{\partial x_i} + e_{ijk} \frac{\partial}{\partial x_i} \bar{S}_{jk} = 0. \tag{16}$$

Since for hexagonal crystals $e_{33k} = 0$ and $e_{3k3} = 0$, unless $k = 3$, we obtain from eq. (16) with the help of eqs. (11) and (12)

$$\frac{\partial \bar{E}_3}{\partial x_3} = \frac{e_{333}}{\epsilon_{33}} \frac{\partial \bar{S}_{33}}{\partial x_3}. \tag{17}$$

From eqs. (15) and (17) we may conclude that

$$\frac{\partial \bar{E}_3}{\partial x_3} = \frac{\partial \bar{S}_{33}}{\partial x_3} = 0. \tag{18}$$

Eq. (18) means among other things that we are dealing with a uniform electric field strength $\bar{E}_3$. Thence $\bar{v}_{d_3}$ is also independent of x_3, so

$$\bar{v}_{d_3} = -\mu_{33}\bar{E}_3 = \mu_{33}\frac{\bar{V}}{L}, \tag{19}$$

where μ_{ij} are the free electron mobility tensor elements and $\bar{V}$ is the voltage applied to the sample. Since we assumed that the donor centres are distributed uniformly throughout the crystal we may put

$$\frac{\partial \bar{n}}{\partial x_i} = 0. \tag{20}$$

Therefore in the stationary state the diffusion contribution to the current density can be omitted. In view of the rotational symmetry with respect to the x_3-axis we can write

$$\frac{\partial \bar{n}_d}{\partial x_i} = \frac{\partial \bar{n}_s}{\partial x_i} = 0, \quad \text{for } i = 1, 2. \tag{21}$$

Combining eqs. (2), (3), (4), (20) and (21) we obtain

$$\bar{v}_{d_3}\frac{\partial \bar{n}_d}{\partial x_3} + \bar{v}_{s_3}\frac{\partial \bar{n}_s}{\partial x_3} = 0. \tag{22}$$

With the help of eqs. (1) and (20), we find from eq. (22)

$$(\bar{v}_{d_3} - \bar{v}_{s_3})\frac{\partial \bar{n}_d}{\partial x_3} = 0. \tag{23}$$

Since $\bar{v}_{d_3} > \bar{v}_{s_3}$ for applied bias in excess of the threshold voltage for amplification, we have [8]

$$\frac{\partial \bar{n}_d}{\partial x_3} = \frac{\partial \bar{n}_s}{\partial x_3} = 0. \tag{24}$$

Note that (24) is also valid for $\bar{v}_{d_3} \leqslant \bar{v}_{s_3}$ because in that case $\bar{n}_s = 0$ and $\bar{n}_d = \bar{n}$.

From the above it is clear that the expression for the current becomes (eqs. (3) and (19))

$$\bar{I} = -qA\,\bar{n}_s\bar{v}_{s_3} - qA\,\bar{n}_d\frac{\mu_{33}\bar{V}}{L}, \tag{25}$$

where A is the contact area.

In earlier reports [8] it was assumed that $\bar{n}_s$ and $\bar{n}_d$ were voltage independent at sufficiently high voltages since the IV-characteristics showed that there was a linear relationship between $\bar{I}$ and $\bar{V}$ in the electro–acoustically active region (cf. eq. (25)). However, if the knee voltage in the IV-characteristic, defined by the intersection of the ohmic straight line with the line mentioned above, does not coincide with the actual threshold voltage for amplification, this approximation is not allowed. In all cases known to the authors the threshold voltage obtained at the onset of electro–acoustic current fluctuations [8] is lower than the knee voltage in the IV-characteristic. This means that $\bar{n}_s$ and $\bar{n}_d$, and their deviations from the stationary state values depend on $\bar{V}$.

From the slope R^{-1} of the IV-characteristic below the threshold voltage we obtain the mean charge carrier density in the conduction band:

$$\bar{n} = \frac{L}{qA\mu_{33}R}. \tag{26}$$

For amplification of an acoustic wave the ratio of the component of the drift velocity in the direction of the sound velocity and the sound velocity has to be larger than unity. This is readily achieved for small off-axis angles. Therefore the threshold voltage for amplification of sound waves V_c in our crystals is determined by the phase velocity of transverse on-axis waves, although the electromechanical coupling of these waves is zero. So we have

$$V_c = \frac{\bar{v}_s \cdot L}{\mu_{33}}. \tag{27}$$

At increasing voltage the off-axis angle of maximum amplification increases until it saturates at 30°, because there is a maximum in the electromechanical coupling factor at 30° [12]. It should be noted that in view of this the trough velocity component along the x_3-axis, $\bar{v}_{s_3}$, used in eq. (25) depends essentially on the applied voltage $\bar{V}$.

When we use eqs. (1), (25) and (26) we find when $\bar{V} > V_c$

$$\bar{n}_s(\bar{V}) = \frac{L}{qA\mu_{33}}\frac{\bar{I} + \bar{V}/R}{(\bar{V} - \bar{v}_{s_3} \cdot L/\mu_{33})}. \tag{28}$$

(Note that $\bar{V}$ and $\bar{I}$ have opposite signs.)
As a consequence of eqs. (1), (26) and (28) $\bar{n}_d(\bar{V})$ is given by

$$\bar{n}_d(\bar{V}) = \frac{L}{qA\mu_{33}}\left[\frac{1}{R} - \frac{\bar{I} + \bar{V}/R}{\bar{V} - \bar{v}_{s_3} \cdot L/\mu_{33}}\right]. \tag{29}$$

2.3. The ac impedance

In the calculation given below we extend Greebe's impedance calculation of piezoelectric plates [10] by including trough creation and annihilation processes [11], and by allowing for off-axis waves.

For small deviations Δ from the stationary state we have in first order approximation

$$\Delta p - \Delta b = -\frac{\Delta n_t}{\tau} + \left(\frac{\partial p}{\partial E_i} - \frac{\partial b}{\partial E_i}\right)_{\Delta E_i = 0} \Delta E_i, \tag{30}$$

with

$$\tau = -\left(\frac{\partial p}{\partial n_t} - \frac{\partial b}{\partial n_t}\right)^{-1}_{\Delta n_t = 0},$$

the mean lifetime of fluctuations in the trough density, where p and b depend explicitly on n_t and E. Now, with help of eq. (30), eq. (9) becomes

$$\frac{\partial \Delta n_t}{\partial t} = -\frac{\Delta n_t}{\tau} + \left(\frac{\partial p}{\partial E_i} - \frac{\partial b}{\partial E_i}\right)_{\Delta E_i = 0} \Delta E_i - v_{s_j} \frac{\partial \Delta n_t}{\partial x_j}. \tag{31}$$

By linearising eq. (3) and using

$$\Delta v_{d_i} = -\mu_{ij} \Delta E_j, \tag{32}$$

and

$$\Delta v_{s_i} = -\mu'_{ij} \Delta E_j, \tag{33}$$

where μ'_{ij} are the mobility tensor elements associated with trapped electrons, we find

$$\Delta j_i = q(\mu_{ij}\bar{n}_d + \mu'_{ij}\bar{n}_s)\Delta E_j + q(\bar{v}_{d_i} - \bar{v}_{s_i})\Delta n_s + qD_{n_{ij}} \frac{\partial \Delta n}{\partial x_j} - q\bar{v}_{d_i} \Delta n + \frac{\partial \Delta D_i}{\partial t}. \tag{34}$$

Eq. (9) becomes

$$\Delta n_s = \bar{N} \Delta n_t + \bar{n}_t \Delta N. \tag{35}$$

In addition we assume that the number of electrons per trough N depends only on the electric field strength; thence

$$\Delta N = \left(\frac{\partial N}{\partial E_j}\right)_{\Delta E_j = 0} \cdot \Delta E_j. \tag{36}$$

Equations (1), (2), (4), (5), (6), (7) and (8) can be expressed in small deviations from the stationary state in a trivial way. Before looking for solutions of our set of equations it will prove useful to study the polarisation of the sound-wave-induced electric field strength [13] and [15]).

When a sound wave moves along a general crystal direction, the local electric field strength can be given by

$$\boldsymbol{E}(x, t) = \bar{\boldsymbol{E}}(x) + \Delta \boldsymbol{E}(x, t), \tag{37}$$

with

$$\Delta \boldsymbol{E}(x, t) = \Delta \boldsymbol{E}_k \, e^{i(\omega t - \boldsymbol{k} \cdot x)},$$

$$\boldsymbol{k} = (k_{RE} + ik_{IM})\kappa.$$

Note that $\boldsymbol{k}$ can be a complex vector, the real part of which ($k_{RE}\kappa$) is the ordinary wave vector, whereas the imaginary part ($k_{IM}\kappa$) describes the amplification of the sound wave. κ is a unit vector in the direction of the wave propagation.

Maxwell's equations yield

$$\nabla \times (\nabla \times \boldsymbol{E}) = -\mu_0 \mu \cdot \frac{\partial}{\partial t} \boldsymbol{j}, \tag{38}$$

where μ_0 is the free space permeability and μ the relative permeability tensor. It should be remembered, that $\boldsymbol{j}$ is the total current density vector. When we assume that $\mu \cdot \boldsymbol{j} = \boldsymbol{j}$, we find the following expression for the time varying electric field component $\Delta \boldsymbol{E}(x, t)$:

$$-k^2 \Delta \boldsymbol{E} + \boldsymbol{k}(\boldsymbol{k} \cdot \Delta \boldsymbol{E}) = -\mu_0 i\omega \Delta \boldsymbol{j}, \tag{39}$$

where $k^2 = (\boldsymbol{k} \cdot \boldsymbol{k})$ and $\Delta \boldsymbol{j}$ is the current density.

If we assume that $|k_{IM}/k_{RE}| \ll 1$, i.e. the amplification is close to unity over one wavelength, and use $\omega^2/k_{RE}^2 = \bar{v}_s^2$, eq. (39) can be rewritten as

$$\Delta E - \kappa(\kappa \cdot \Delta E) = (\bar{v}_s)^2 \cdot \frac{i\mu_0 \Delta j}{\omega}. \tag{40}$$

The left hand side of eq. (40) yields the transverse component of ΔE. To estimate the order of magnitude of the transverse component of ΔE it is convenient to replace Δj by $\sigma \Delta E$, where σ is a typical conductivity for the samples under study. Eq. (40) now becomes:

$$\frac{|\Delta E - \kappa(\kappa \cdot \Delta E)|}{|\Delta E|} = (\bar{v}_s)^2 \frac{\mu_0 \sigma}{\omega}. \tag{41}$$

It can be shown that in all practical cases the magnitude of the transverse electric field component can be neglected with respect to $|\Delta E|$ if reasonable values for the unknowns are inserted into the right hand side of eq. (41). (For example we used $\bar{v}_s = 2 \times 10^3$ ms^{-1}, $\mu_0 = 1.26 \times 10^{-6}$ H m^{-1}, $\sigma < 100$ $(\Omega$ m$)^{-1}$ and $\omega > 10^5$ s^{-1}.)
Therefore for the acoustic-wave-induced electric field strength we may write

$$\Delta E = \Delta E \cdot \kappa. \tag{42}$$

From eq. (8) we obtain the strain tensor elements

$$\Delta S_{ij} = \tfrac{1}{2} \Delta S(\pi_i \kappa_j + \pi_j \kappa_i), \tag{43}$$

where π is a unit vector along the direction of the acoustic polarisation and ΔS is a scalar strain amplitude.

Equations (1), (2), (4)–(8), (31), (34)–(36) form a set of 11 linear homogeneous differential equations in 11 variables, ΔT, ΔS, ΔE, ΔD, ΔN, Δu, Δj, Δn_t, Δn_s, Δn_d and Δn, which can be solved by considering solutions of the type $\exp i(\omega t - k \cdot x)$. When $k = 0$ we find a trivial solution. After some algebra the dispersion relation for $k \neq 0$ becomes, when eqs. (42) and (43) are used (note that i when not used as a subscript is the imaginary unity):

$$\rho\omega^2 = c^{*\prime} k^2, \tag{44}$$

where

$$c^{*\prime} = c^*[1 + K_e^{*2}\beta^*],$$

$c^* = \kappa_i \pi_j c_{ijkl} \pi_k \kappa_l$, the effective elastic constant,

$e^* = \kappa_i e_{ijk} \pi_j \kappa_k$, the effective piezoelectric constant (We used $e_{ijk} = e_{ikj}$ in hexagonal crystals.),

$\epsilon^* = \kappa_i \epsilon_{ij} \kappa_j$, the effective dielectric constant,

$K_e^* = \left[\frac{(e^*)^2}{\epsilon^* c^*}\right]^{\frac{1}{2}}$, the effective electromechanical coupling factor.

$$\beta^* = \left[1 + \frac{\alpha^*(1/\tau + i(\omega - k\bar{v}_s))^{-1} + \sigma_1^* + \sigma_2^* + \sigma_3^*}{\epsilon^*(k^2 D_n^* + i(\omega - k\bar{v}_{d_i}\kappa_i))}\right]^{-1},$$

$$\alpha^* = -q\bar{v}_s \gamma^* \bar{N} \left\{ \left(\frac{\partial p}{\partial E_i} - \frac{\partial b}{\partial E_i} \right)_{\Delta E_i = 0} \cdot \kappa_i \right\},$$

$\gamma^* = 1 - \frac{\bar{v}_{d_i}\kappa_i}{\bar{v}_s}$, the effective drift parameter,

$\mu^* = \kappa_i \mu_{ij} \kappa_j$, $\mu'^* = \kappa_i \mu'_{ij} \kappa_j$, $\sigma_1^* = q\mu^* \bar{n}_d$,

$\sigma_2^* = q\mu'^* \bar{n}_s$,

$$\sigma_3^* = -q\bar{v}_s \gamma^* \bar{n}_t \left\{ \left(\frac{\partial N}{\partial E_i} \right)_{\Delta E_i = 0} \cdot \kappa_i \right\},$$

$D_n^* = \kappa_i D_{n_{ij}} \kappa_j$, the effective diffusion constant.

From eq. (44) we see that all electro-acoustic effects on wave propagation are described by a new elastic constant $c^{*\prime}$. The solution of eq. (44) can now be simplified if it is assumed that the coupling between the acoustic waves and the electrons is small; in other words the electronic amplification will not change the acoustic wave amplitudes by more than a few per cent over one wavelength.
Accordingly we assume that

$$|K_e^{*2}\beta^*| \ll 1. \tag{45}$$

Since β^* is still unknown, condition (45) should be verified later on for consistency. This small coupling

approximation implies that $c^{*\prime}$ (and therefore k as well) contains a small imaginary part. When condition (45) holds, eq. (44) becomes a quadratic equation in k with solutions (we used $\bar{v}_s = (c^*/\rho)^{1/2}$) given by

$$k = k_1 \approx \frac{\omega}{\bar{v}_s}(1 - \tfrac{1}{2}K_e^{*2}\beta_1^*),$$

and

$$k = k_2 \approx -\frac{\omega}{\bar{v}_s}(1 - \tfrac{1}{2}K_e^{*2}\beta_2^*). \tag{46}$$

Note that the terms $K_e^2\beta_{1,2}^*$ are not neglected with respect to unity because they contain a small imaginary part.

Setting $k_1 \approx \omega/\bar{v}_s$ in β_1^* and $k_2 \approx -\omega/\bar{v}_s$ in β_2^*, and introducing the angular diffusion frequency $\omega_D^* = \bar{v}_s^2/D_n^*$ we find

$$\beta_1^* = \left(\gamma^* - i\frac{\omega}{\omega_D^*}\right) \Bigg/ \left[\gamma^* - i\left(\frac{\omega}{\omega_D^*} + \frac{\alpha^*\tau + \sigma_1^* + \sigma_2^* + \sigma_3^*}{\epsilon^*\omega}\right)\right]$$

and

$$\beta_2^* = \left(2 - \gamma^* - i\frac{\omega}{\omega_D^*}\right) \Bigg/ \left[2 - \gamma^* - i\left(\frac{\omega}{\omega_D^*} + \frac{\alpha^*(1/\tau + 2i\omega)^{-1} + \sigma_1^* + \sigma_2^* + \sigma_3^*}{\epsilon^*\omega}\right)\right] \tag{47}$$

Now that we have found the dispersion relations, the solution of our basic equations for any variable $\Delta y(x, t)$ at fixed angular frequency ω can be written as a linear combination of plane waves with wave numbers $k = 0$ representing a solution with no position dependence, $k = k_1$ representing a plane wave travelling along κ and $k = k_2$ representing a plane wave travelling in the opposite direction. So in general we have

$$\Delta y(x, t) = y_0 e^{i\omega t} + y_1 e^{i(\omega t - k_1 \cdot x)} + y_2 e^{i(\omega t - k_2 \cdot x)}, \tag{48}$$

where Δy, y_0, y_1 and y_2 are tensor, vector, or scalar quantities. It should be noted that the result obtained describes only the behaviour of off-axis waves with wave vector direction κ. In practice, however, we shall deal with a distribution of off-axis angles. In section 4 we shall discuss the effects of this distribution.

We shall first return to our basic equations to derive some useful relations between the plane wave amplitudes of our variables for each mode separately. When $k = 0$ it follows from eqs. (8), (42) that

$$S_0\pi_i\kappa_j = 0, \tag{49}$$

from eqs. (6), (42), (49) that

$$\kappa_i D_{0_i} = \epsilon^* E_0, \quad \text{where } E_{0_i} = E_0\kappa_i, \tag{50, 51}$$

from eqs. (5), (49) that

$$\pi_i\kappa_j T_{0_{ij}} = -e^* E_0, \tag{52}$$

and from eqs. (31)–(36), (44) and (50) that

$$j_{0_i} = [\alpha^*(1/\tau + i\omega)^{-1} + \sigma_1^* + \sigma_2^* + \sigma_3^*]E_0\kappa_i. \tag{53}$$

When $k = k_1$ or $k = k_2$ we find from eqs. (5), (7), (8) and (44) that

$$\pi_i\kappa_j(T_{1,2})_{ij} = -\frac{e^*}{\beta_{1,2}^* K_e^{*2}} E_{1,2}, \tag{54}$$

and from eq. (4) that

$$(j_{1,2})_i = 0. \tag{55}$$

The choice of boundary conditions allows us to determine the relative magnitudes of the three modes (cf. eq. (48)). For free end-surfaces it is convenient to take the boundary conditions to be:

$$\pi_i\kappa_j\{(T_0)_{ij} + (T_1)_{ij} e^{-ik_1 \cdot x} + (T_2)_{ij} e^{-ik_2 \cdot x}\} e^{i\omega t} = 0, \tag{56}$$

at the cathode, $x = 0$, and at the anode $x = L'\kappa$, where $L' = L/(\kappa \cdot e_3)$ and e_3 is a unit vector along the x_3-axis. When we use eqs. (52) and (54) we obtain from eq. (56)

$$E_1 = K_e^{*2}\beta_1^*\left[\frac{e^{-ik_2L'} - 1}{e^{-ik_1L'} - e^{-ik_2L'}}\right] \cdot E_0,$$

and

$$E_2 = -K_e^{*2}\beta_2^*\left[\frac{e^{-ik_1L'} - 1}{e^{-ik_1L'} - e^{-ik_2L'}}\right] \cdot E_0. \quad (57)$$

The alternating voltage with angular frequency ω developed along the x_3-axis is given by

$$\Delta V = -\int_0^L [E_0 + E_1 e^{-ik_1 \cdot x} + E_2 e^{-ik_2 \cdot x}] e^{i\omega t} \kappa_3 dx_3, \quad (58)$$

where x_3 is the position at the x_3-axis and

$$x = \frac{x_3 \cdot \kappa}{\kappa \cdot e_3}. \quad (59)$$

From eqs. (53), (57), (58) and (59) we finally obtain the ac small signal impedance at angular frequency ω:

$$Z(\omega) = \frac{L}{A(\alpha^*/(1/\tau + i\omega) + \sigma_1^* + \sigma_2^* + \sigma_3^* + i\omega\epsilon^*)} \times \left\{1 + \frac{K_e^{*2}(e^{-ik_1L'} - 1)(e^{-ik_2L'} - 1)(ik_1\beta_2^* - ik_2\beta_1^*)}{L'k_1k_2(e^{-ik_1L'} - e^{ik_2L'})}\right\}. \quad (60)$$

Substituting reasonable values for the unknowns in eq. (60) it is found that the term containing K_e^{*2} only contributes significantly at frequencies given by

$$f = (2m + 1)\frac{\bar{v}_s}{2L'}, \quad m = 0, 1, 2, 3, \ldots. \quad (61)$$

Note that $L'/\bar{v}_s$ is the transit time of the sound waves.

Three limiting cases are of interest for our measurements (i) $\omega \to 0$; then eq. (60) becomes

$$Z(0) = \frac{L}{A(\alpha^*\tau + \sigma_1^* + \sigma_3^*)}. \quad (62)$$

(σ_2^* vanishes, because μ_{ij}' is assumed to go to zero when $\omega \to 0$.)

(ii) $$\omega \gg \left|\frac{\sigma_1^* + \sigma_2^* + \sigma_3^* + \alpha^*/(1/\tau + i\omega)}{\epsilon^*}\right|; \quad (63)$$

then

$$Z(\omega) \approx \frac{L}{iA\epsilon^*\omega}, \quad (64)$$

which corresponds to the dielectric roll-off of a device with capacity $C = \epsilon^*A/L$.

(iii) intermediate frequencies, where

$$\sigma_1^* + \sigma_2^* + \sigma_3^* \gg \left| i\omega\epsilon^* + \frac{\alpha^*}{(1/\tau + i\omega)}\right|.$$

Then we find an impedance which is given by

$$Z(\omega) = \frac{L}{A(\sigma_1^* + \sigma_2^* + \sigma_3^*)}. \quad (65)$$

2.4. Additional results

Although the main purpose of this section was to calculate the ac-impedance, it should be noted that one can obtain some other interesting results. The imaginary parts of k_1 and k_2 (cf. eq. (46)) yield the attenuation coefficients α_{e_1} of waves travelling to the anode and α_{e_2} of waves travelling in the opposite direction, respectively. In fact it turns out that

$$\alpha_{e_1}(\omega) = -\text{im}\,(k_1) = \frac{K_e^{*2}(\alpha^*\tau + \sigma_1^* + \sigma_2^* + \sigma_3^*)\gamma^*}{2\bar{v}_s\epsilon^*} \times \left[\gamma^{*2} + \left(\frac{\omega}{\omega_D^*} + \frac{\alpha^*\tau + \sigma_1^* + \sigma_2^* + \sigma_3^*}{\epsilon^*\omega}\right)^2\right]^{-1}, \quad (66)$$

and that

$$\alpha_{e_2}(\omega) = \text{im}\,(k_2) = \frac{K_e^{*2}(\alpha^*\tau/(1 + 4\omega^2\tau^2) + \sigma_1^* + \sigma_2^* + \sigma_3^*)}{2\bar{v}_s\epsilon^*} \times \left(2 - \gamma^* - \frac{2\alpha^*\tau^2}{\epsilon^*(1 + 4\omega^2\tau^2)}\right)$$

$$\times \left[\left(2-\gamma^*-\frac{2\alpha^*\tau^2}{\epsilon^*(1+4\omega^2\tau^2)}\right)^2 + \left(\frac{\omega}{\omega_D^*}+\frac{\alpha^*\tau/(1+4\omega^2\tau^2)+\sigma_1^*+\sigma_2^*+\sigma_3^*}{\epsilon^*\omega}\right)^2\right]^{-1}. \quad (67)$$

These expressions reduce to White's result for the linear attenuation coefficient [2], when we choose $\alpha^* \cdot \tau = 0$ and replace $\sigma_1^* + \sigma_2^* + \sigma_3^*$ by the conductivity σ.

From eq. (66) we see directly that α_{e_1} is negative (amplification) if $\gamma^* < 0$, i.e. $\bar{v}_d > \bar{v}_s/\kappa_3$ (experimental results show that the term $(\alpha^*\tau + \sigma_1^* + \sigma_2^* + \sigma_3^*)$ is always positive). From eq. (67) we find that α_{e_2} is positive (attenuation) if $\gamma^* < 2 - (2\alpha^*\tau^2)/\{\epsilon^*(1+4\omega^2\tau^2)\}$ (the term $(\alpha^*\tau/(1+4\omega^2\tau^2) + \sigma_1^* + \sigma_2^* + \sigma_3^*)$ is always positive. Since the experiments show that $\alpha^* < 0$ (cf. section 4) it follows that in all cases where troughs are present ($\bar{v}_d > \bar{v}_s/\kappa_3$) α_{e_2} is positive, i.e. back-travelling waves are always attenuated.

As a final result we mention the frequency of maximum amplification of waves travelling to the anode, f_m, which can be obtained from eq. (66)

$$f_m = \frac{1}{2\pi} \cdot \left[\omega_D^* \cdot \frac{\alpha^*\tau + \sigma_1^* + \sigma_2^* + \sigma_3^*}{\epsilon^*}\right]^{1/2}. \quad (68)$$

The frequency of maximum attenuation for waves travelling to the cathode is more complicated to derive and will not be discussed here.

Since the term $\alpha^*\tau + \sigma_1^* + \sigma_2^* + \sigma_3^*$ is allowed to depend on the applied voltage, f_m is allowed to be voltage dependent as well. It seems very likely that the downshift of f_m at increasing bias voltage as reported by several authors (cf. [16]) can be interpreted in terms of eq. (68). The most interesting feature is that f_m can be determined with the help of parameters obtained from ac impedance measurements.

3. Experimental arrangement

We used semiconducting CdS single crystals with a resistivity of 0.3 Ω m provided by the Eagle Picher Company. Measurements were done in the longitudinal configuration ($\boldsymbol{E}\|c$-axis).

Before evaporating indium onto the contact faces, we polished the two contact faces mechanically within 0.25 μm. Two opposite side faces were polished as well to enable us to carry out Brillouin scattering experiments on these crystals at a later stage.

Thin copper wires were ultrasonically soldered to the contacts.

The contact spacing L and contact area A of the samples were as follows:

Sample I: $L = 1.53 \times 10^{-3}$ m;
$A = 1.00 \times 0.80 \times 10^{-6}$ m^2,
Sample II: $L = 1.40 \times 10^{-3}$ m;
$A = 1.00 \times 0.72 \times 10^{-6}$ m^2.

The sample lengths were kept smaller than 2×10^{-3} m to suppress electro–acoustic domain formation, which would give rise to a highly nonlinear electric field distribution in the samples [7].

To avoid Joule heating of the samples the high voltage was applied in pulses of 40 μs with a repetition rate of 4 Hz. These pulse lengths, which were much longer than the transit times of acoustic waves (≈ 1 μs), allowed the samples to reach a stationary state.

The experimental set-up for the impedance measurements is shown in fig. 1.

The low pass filter was used to suppress the higher harmonics of the voltage pulse, whereas the high pass filter protected the sine wave generator output stage against remaining transients of the voltage pulse. These filters limited the frequency range for impedance measurements to frequencies above 400 kHz. The high frequency limit for impedance measurements turned out to be 100 MHz. This value was determined by the metal film resistors which were used for reference and by parasitic capacitances.

To suppress the huge broad-band noise generated by the electro–acoustic effect we used a HP 8558 B spectrum analyser (input resistance 50 Ω) as a band pass filter with a bandwidth of 300 kHz at low frequencies and a bandwidth of 1 MHz at high frequencies. The IF-output (21.4 MHz) of the spectrum analyser was fed into a switch which only transmitted the signal between 5 and 35 μs after the onset of the bias pulse. The transmitted power was measured with an HP 435 A power meter.

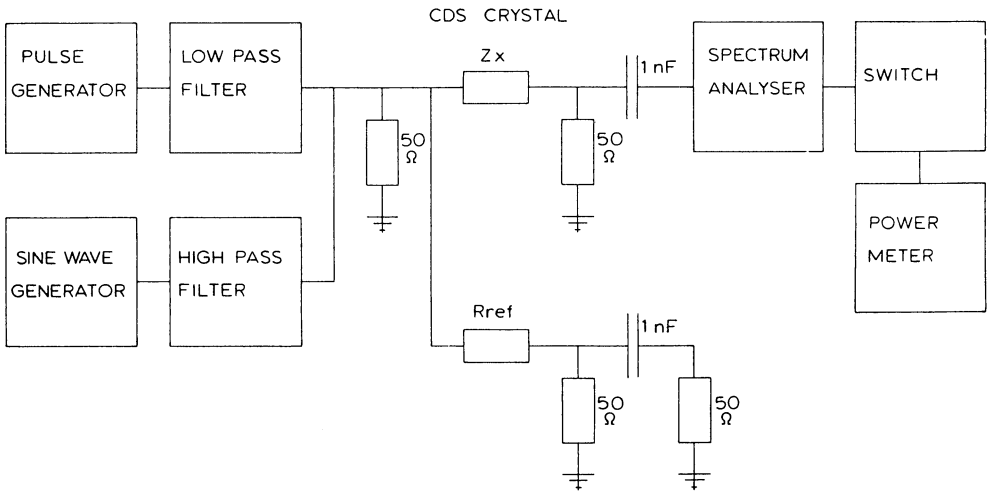

Fig. 1. Experimental set-up for measurements of the absolute value of the impedance under pulsed bias conditions.

To determine the absolute value of the ac impedance of the samples, we measured the power meter deflection with the sine wave generator switched on (P_1) and the background power (P_2) caused by electro–acoustic current fluctuations and the equivalent input noise of our measuring circuit in the absence of the sine wave signal. Thereupon we interchanged Z_x and R_{ref} and measured P_3 (sine wave generator switched on) and background P_4 (sine wave generator switched off). If $|Z_x|$ and R_{ref} (which was always chosen to be of the same order of magnitude as $|Z_x|$) are large compared to 25 Ω, it can be shown that Z_x is given by:

$$|Z_x|^2 \simeq \frac{P_3 - P_4}{P_1 - P_2} \cdot R_{ref}^2. \tag{69}$$

4. Results and discussion

Fig. 2 shows the current voltage characteristic of sample II. At low voltages the sample is ohmic, at about 130 V the current starts to deviate from the

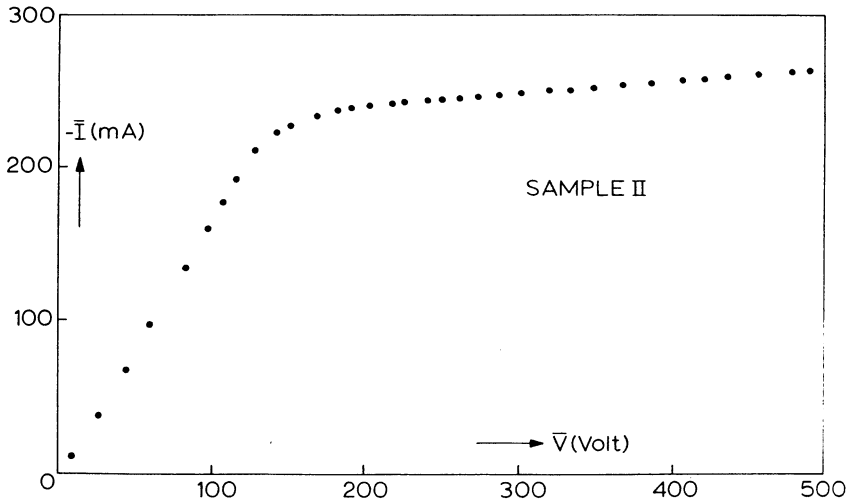

Fig. 2. Current–voltage characteristic of sample II.

ohmic behaviour and at voltages above 190 V we obtain a linear relationship between $\bar{I}$ and $\bar{V}$ (cf. section 2). Similar results were obtained for sample I. The observed linear relationship at high voltages between $\bar{I}$ and $\bar{V}$ yields

$$-\bar{I} = -I_0 + \frac{\bar{V}}{R_d}, \tag{70}$$

where $1/R_d$ is the slope of the curve at high voltages and $-I_0$ the extrapolated intersection with the current axis. Inserting eq. (70) into eq. (28) we find that at high voltages the voltage dependence of $\bar{n}_s(\bar{V})$ is given by

$$\bar{n}_s(\bar{V}) = \frac{L}{qA\mu_{33}} \frac{I_0 + \bar{V}(1/R - 1/R_d)}{\bar{V} - \bar{v}_{s_3} L/\mu_{33}}. \tag{71}$$

When we define the knee voltage V_k as the intersection of the ohmic curve with the curve given by eq. (70), eq. (56) can be rewritten as

$$\bar{n}_s(\bar{V}) = \frac{L}{qA\mu_{33}} \frac{R_d - R}{R_d R} \frac{\bar{V} - V_k}{\bar{V} - \bar{v}_{s_3} L/\mu_{33}}. \tag{72}$$

From this equation it is obvious that $\bar{n}_s(\bar{V})$ becomes voltage independent, when V_k coincides with $\bar{v}_{s_3} L/\mu_{33}$.

Note that from eq. (27) it follows that $\bar{v}_{s_3} L/\mu_{33} \leqslant V_c$ always.

Earlier reports [9] showed that the knee voltage V_k in the *IV* characteristic is in most cases somewhat higher than the voltage defined by the onset of the electro–acoustic current fluctuations V_c. We therefore measured the power of the current fluctuations as a function of the applied voltage and extrapolated the electro–acoustic current fluctuations to the thermal current noise level [9] in order to determine the threshold voltage V_c.

For our samples V_c appeared to be about 0.8 times V_k, which means that $\bar{n}_s(\bar{V})$ is voltage dependent. However, so far we have no physical explanation for the voltage dependence of $\bar{n}_s(\bar{V})$, given in eq. (71), or rather for the observed linear *IV* characteristic at high voltages (cf. eq. (70)).

For sample I we obtained $V_c = 125$ V. When we use the sound velocity of transversal on-axis waves $\bar{v}_s = 1.8 \times 10^3$ m s^{-1}, we obtain with the help of eq. (27) $\mu_{33} = 2.20 \times 10^{-2}$ m^2 V^{-1} s^{-1}, which is in good agreement with the reported value of the mobility in the literature [17]. Sample II showed the same result within 10%.

From the threshold voltage, from the *IV* characteristic and from Brillouin scattering data as well it was clear that only transversal acoustic waves were amplified. From the *IV* characteristics and the threshold voltages obtained we could calculate the quantity $\bar{n}_s(\bar{V})$ with the help of eq. (28).

In fig. 3 the quantity $\bar{n}_s/\bar{n}$ is plotted as a function of $\bar{V}/V_c$ for sample II. We used $\mu_{33} = 2.2 \times 10^{-2}$ m^2 V^{-1} s^{-1} and $\bar{v}_s = 1.8 \times 10^3$ m s^{-1}. Furthermore it was assumed that the off-axis angle was 30°, an assumption that is certainly not valid when $(\bar{V} - V_c)/V_c \ll 1$ [12]. Consequently the calculated values of $\bar{n}_s/\bar{n}$ will be a little too small when $(\bar{V} - V_c)/V_c \ll 1$. However, this approximation will not alter the qualitative interpretation of fig. 3. The trapping starts at voltages close to V_c; with increasing voltage the acoustic energy density increases, causing more electrons to become trapped in potential troughs. From eqs. (26) and (72) we can deduce the saturation value of $\bar{n}_s/\bar{n}$ for $\bar{V} \to \infty$:

$$\lim_{\bar{V}\to\infty} \frac{\bar{n}_s(\bar{V})}{\bar{n}} = \frac{R_d - R}{R_d}. \tag{73}$$

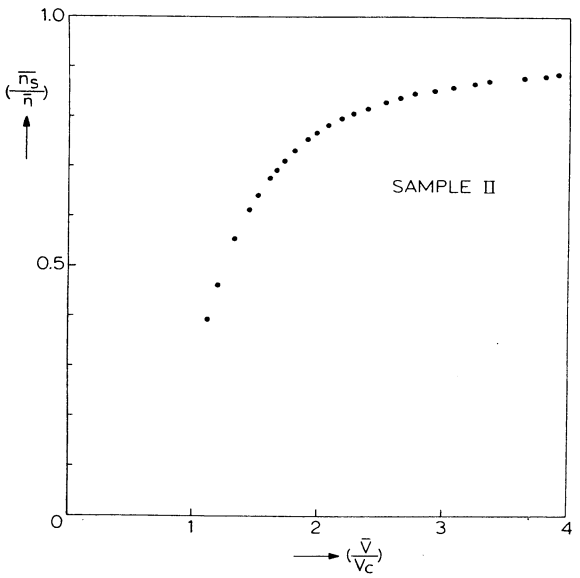

Fig. 3. Relative trapped electron density $\bar{n}_s/\bar{n}$ as a function of $\bar{V}/V_c$ for sample II.

From fig. 2 we find for sample II a saturation value of 0.95. Sample I shows a similar behaviour, and also has a saturation value of 0.95.

Fig. 4 shows the result of an impedance measurement at 150 V for sample I as a function of frequency. Besides the low frequency roll-off, we observe resonances which appear at frequencies given by the odd harmonics of 500 kHz. Since transverse off-axis waves with wave vectors making an angle from 10° to 50° with the direction of the electric field strength (or the c-axis) are expected to be amplified [12], the resonances predicted by eq. (61) will be smoothed out over a larger frequency interval. This smoothing out will occur because in practice we have a distribution of trough velocities which corresponds with a distribution of transit times. This explains why the observed resonances are much wider than those given by eq. (61). From eq. (61) we find an off-axis angle of 32° (we used $\bar{v}_s = 1.8 \times 10^3$ m s^{-1}).

The solid line in fig. 4 is calculated with the help of eq. (60). An unambiguous fit to the measurements can be obtained by taking $\tau = 1.79 \times 10^{-7}$ s, $\alpha^* = -5.77 \times 10^6$ $(\Omega$ m s$)^{-1}$ and $\sigma_1^* + \sigma_2^* + \sigma_3^* = 2.77$ $(\Omega$ m$)^{-1}$. It should be noted that in eq. (60) we assumed that μ'^* is a constant in the frequency range considered (in fact observing an impedance plateau at intermediate frequencies eq. (64) yields μ'^* is a constant at intermediate frequencies).

From the IV characteristic we find with eq. (29) at 150 V $\bar{n}_d = 7.6 \times 10^{20}$ m^{-3}, so $\sigma_1^* = 2.66$ $(\Omega$ m$)^{-1}$, and with eq. (28) $\bar{n}_s = 1.8 \times 10^{20}$ m^{-3}. From eq. (62) and the differential resistance in the IV characteristic $|Z(0)|$ at 150 V we obtain

$$\sigma_3^* = \frac{L}{A|Z(0)|} - \alpha^*\tau - \sigma_1^* = -0.35\ (\Omega\ \mathrm{m})^{-1}.$$

It follows therefore that $\sigma_2^* = 0.46$ $(\Omega$ m$)^{-1}$, which means that $\mu'^* = 1.6 \times 10^{-2}$ m^2 V^{-1} s^{-1}.

However, we must realize that the low frequency roll-off is obscured somewhat by the resonances. When we estimate the uncertainty in the product $\alpha^*\tau$ to be around 20% for this case and the uncertainty in $|Z(0)|$ and σ_1^* to be 10%, the error in σ_3^* becomes 106% and in σ_2^* and μ'^* 100%. Thus, it is obvious that one should be careful in drawing quantitative conclusions from the above.

Fig. 5 shows the ac impedance at 184 V for sample II. Again we observe a low frequency roll-off and resonances. The resonances obviously are the odd harmonics of 560 kHz and yield with eq. (61) an off-axis angle of 29°, which is in good agreement with the

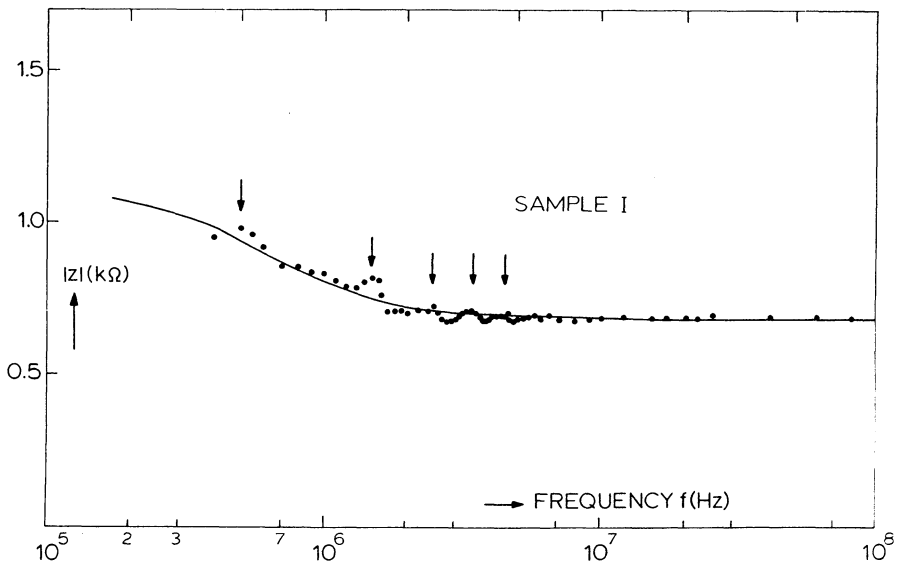

Fig. 4. The absolute value of the ac impedance Z of sample I at 150 V ($\gamma^* = -0.014$). The solid line gives the best fit impedance calculated with the help of eq. (60). Resonance frequencies are indicated by arrows.

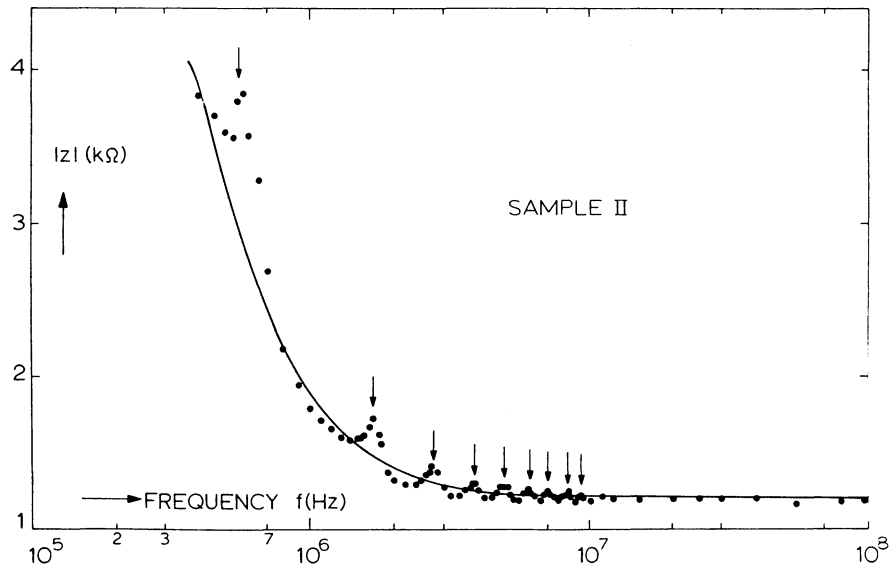

Fig. 5. The absolute value of the ac impedance Z of sample II at 184 V ($\gamma^* = -0.41$). The solid line gives the best fit impedance calculated with the help of eq. (60). Resonance frequencies are indicated by arrows.

result obtained for sample I. The solid line was calculated with eq. (60) using $\tau = 1.29 \times 10^{-7}$ s, $\alpha^* = -1.25 \times 10^7$ $(\Omega\ \mathrm{m\ s})^{-1}$ and $\sigma_1^* + \sigma_2^* + \sigma_3^* = 1.62$ $(\Omega\ \mathrm{m})^{-1}$. From the IV characteristic we find at 184 V: $\bar{n}_d = 4.4 \times 10^{20}$ m^{-3}, $\sigma_1^* = 1.56$ $(\Omega\ \mathrm{m})^{-1}$, $\bar{n}_s = 4.9 \times 10^{20}$ m^{-3} and $\sigma_3^* = 1.8 \times 10^{-2}$ $(\Omega\ \mathrm{m})^{-1}$. Consequently we find $\sigma_2^* = 4.2 \times 10^{-2}$ $(\Omega\ \mathrm{m})^{-1}$ and $\mu'^* = 5.35 \times 10^{-4}$ m^2 V^{-1} s^{-1}. When we estimate the error in $\alpha^*\tau$ to be around 20% for this case, the error in $|Z(0)|$ to be 5% and in σ_1^* to be 10%, it follows that the error in σ_3^* is around 700% and in σ_2^* and μ'^* 500%.

Additional impedance measurements were done on samples with contact spacings which were significantly different from those of the samples I and II. These experiments again yielded off-axis angles of about 30°, which is a further experimental affirmation of the present theory.

From our experimental data it was obvious that in all cases condition (45) was fulfilled.

A value of $\alpha^* < 0$ has the physical meaning that an increase in the applied voltage causes an increase in the number of troughs, whereas a value of $\sigma_3^* > 0$ means that the number of electrons per trough decreases when the applied voltage is increased.

Impedance measurements at voltages below V_c showed a constant ac impedance equal to the ohmic resistance obtained from the IV characteristic, at all frequencies.

From our experimental results it was obvious that $(-\alpha^*\tau)$ increased continuously when the bias voltage was increased. From eq. (68) we see that because $\alpha^*\tau < 0$ the frequency of maximum amplification f_m will continuously shift towards lower frequencies with increasing voltage. The authors believe that the down-shift of f_m as a result of parametric down-conversion of interacting waves [15] can be explained by the present theory and can be related to the frequency dependence of the ac impedance.

More experimental data are necessary to complete the physical picture of the voltage dependence of the introduced variables and the relation between impedances and frequency down-conversion of acoustic waves. However, it is clear that problems concerning the ac small signal impedance can be understood in a very simple way.

Acknowledgement

This work was performed as part of the research programme of the "Stichting voor Fundamenteel Onderzoek der Materie" (F.O.M.) with financial support

from the "Nederlandse Organisatie voor Zuiver-Wetenschappelijk Onderzoek" (Z.W.O.).

References

[1] A. R. Hutson, J. M. McFee and D. L. White, Phys. Rev. Lett. 7 (1961) 237.
[2] D. L. White, J. Appl. Phys. 33 (1962) 2547.
[3] W. Wettling and M. Bruun, Phys. Stat. Sol. 34 (1966) 221.
[4] M. Terai and M. Miya, Jap. J. Appl. Phys. 6 (1967) 896.
[5] G. Johri and H. N. Spector, Phys. Rev. B 14 (1977) 4955.
[6] P. K. Tien, Phys. Rev. 171 (1968) 970.
[7] A. R. Moore, J. Appl. Phys. 38 (1967) 2327.
[8] R. J. J. Zijlstra and P. A. Gielen, Physica 95B (1978) 190.
[9] P. A. Gielen and R. J. J. Zijlstra, Physica 95B (1978) 347.
[10] C. A. A. J. Greebe, Philips Res. Repts. 20 (1965) 1.
[11] W. Westera, R. J. J. Zijlstra and M. A. van Dijk, Phys. Lett. 78A (1980) 371.
[12] A. R. Moore, R. W. Smith and P. Worcester, IBM J. Res. Developm. 13 (1969) 503.
[13] N. I. Meyer and M. H. Jørgensen, Festkörperprobleme X, O. Madelung, ed. (Pergamon Vieweg, 1970) p. 21.
[14] D. Berlincourt, H. Jaffe and L. R. Shiozawa, Phys. Rev. 129 (1963) 1009.
[15] A. R. Hutson and D. L. White, J. Appl. Phys. 33 (1962) 40.
[16] B. W. Hakki and R. W. Dixon, Appl. Phys. Lett. 14 (1969) 185.
[17] W. W. Spear and J. Mort, Phys. Soc. Proc. 81 (1963) 130.